Supporting Information for:

Progressive Polar Alignment of Λ-shaped Basic-Building Units within Transition-Metal Oxide Fluoride Materials.

Michael Holland[†,‡] , Martin D. Donakowski[†,‡], Eric Pozzi[†], Andrew Rasmussen[†], Thanh Thao Tran[§], Shannon E. Pease-Dodson[†], P. Shiv Halasyamani[§,‖], Tamar Seideman[†],Rick Van Duyne[†], Kenneth R. Poeppelmeier[†,]*

[†] Department of Chemistry, Northwestern University, 2145 Sheridan Rd., Evanston, IL 60628-3113

‡These authors contributed equally and are co-first-authors.

[§] Department of Chemistry, University of Houston, 136 Fleming Building, Houston, Texas 77204-5003

‖ Department of Chemistry, Aalto University, Laboratory of Inorganic Chemistry, P.O. Box 16100, FI-00076 AALTO, Finland

* Corresponding author. E-mail: krp@northwestern.edu

Contents:

1. A Summary of Compounds 1-8.

Formula	Compound	Spacegroup
$K_{30}(V_2O_2F_9)_9F_2Cl$	1	$P\bar{3}m1$
$K_{10}(V_2O_2F_9)_3Br_2$	2	$C2/m$
$K_{10}(Mo_2O_4F_7)_3Cl$	3	$Pmn2_1$
$K_{10}(Nb_2O_2F_9)_3Br$	4	$Pmn2_1$
$K_{10}(Nb_2O_2F_9)_3Br_{2/2}$	5	$Pmn2_1$
$K_{10}(Mo_2O_4F_7)_3Br_{2/2}$	6	$Pmn2_1$
$K_{10}(Nb_2O_2F_9)_3I_{2/2}$	7	$Pmn2_1$
$K_{10}(Mo_2O_4F_7)_3I_3$	8	$Pmn2_1$

2. Discussion of Resonance Raman Spectroscopy.

Features observed near 220 cm^{-1} in resonance Raman spectra of Compounds **2**, **5**, and **6** may be explainable through bond length asymmetry in the tribromide anions present. Previous work suggests that there is a continuous range of bond length asymmetry possible for Br_3^- in different environments and that as this asymmetry becomes large, v_1 is observed to blue shift and decrease in intensity while the asymmetric stretch (v_2) in the low 200 cm^{-1} region emerges and red shifts.[1,2] The v_2 mode is solely IR active for symmetric trihalides but becomes Raman active with increasing asymmetry.[3,4]

Crystal structures of Compounds **5** and **6** indicate Br_3^- interatomic distance differences of at least 18 pm, consistent with observed v_2 frequencies near 220 cm^{-1}.[1,2] Compared to the similarly asymmetric Br_3^- in $CsBr_3$,[2] red-shifted v_1 bands observed in our spectra may be an effect of the local environment of Br_3^- or may indicate the coexistence of symmetrical Br_3^- species in each compound. On the other hand, the crystal structure of Compound **2** does not reveal Br_3^- asymmetry. In this structure asymmetric Br_3^- may exist as a minority species in accordance with the observed spectrum.

Crystallography revealed analogous I_3^- asymmetry in Compounds **7** and **8**, though to a smaller degree than the bromine-containing compounds. I_3^- bond length differences were calculated to be between 5 and 10 pm in these structures, which may be insufficient in order to observe v_2 as a prominent feature. We acknowledge the possibility that the shoulder observed on the high-wavenumber side of v_1 is v_2 and that it is visible but weak due to the small degree to which I_3^- is asymmetric in these structures.

Alternatively, the peaks at around 220 cm^{-1} in the bromine-containing compounds presented here may be feasibly explained by the presence of bromine chains of lengths other than three atoms. In Raman spectra of Br_5^-, Chen *et al.*[5] observed a terminal asymmetric stretch at 210 cm^{-1} accompanied by a terminal symmetric stretch at 253 cm^{-1}. Since band frequency and intensity may be altered by its degree

of asymmetry, peaks observed in our spectra may be attributable to Br_5^-. However, given our crystallographic data and the absence of a peak near 253 cm^{-1} in our spectra, we do not believe Br_5^- is present in our synthesized compounds. Iqbal *et al*.[6] and Burns and Renner[1] attributed peaks at 230 cm^{-1} and 234 cm^{-1}, respectively, in resonance Raman spectra of compounds containing Br_3^- to the presence of interstitial Br_2 and that its vibrational frequency was shifted in comparison to that of crystalline bromine due to the local environment in each case. This possibility is also unlikely for the compounds presented in this work because of the presented crystallographic structures.

3. Powder X-Ray Diffraction Patterns.

Powder X-Ray Diffraction patterns were collected at room temperature with the use of a Rigaku XDS 2000 with Ni-filtered Cu Kα radiation (λ=1.5418 Å) and compared against patterns in the Joint Committee of Powder Diffraction Standards (JCPDS) database. The red "X" indicates an impurity. For Compound 1, the impurity is Potassium Vanadium Oxide Fluoride ($K_2VF_3O_2$). For Compound 2, the impurities are Vanadium Oxide Fluoride (VOF) and Potassium Bromide Fluoride ($KBrF_6$). For Compound 3, the impurities are Molybdenum Oxide Fluoride ($MoOF_4$) and Potassium Molybdenum Oxide ($K_2Mo_3O_{10}$). For Compound 4, the impurities are Potassium Niobium Fluoride (K_2NbF_7) and Niobium Oxide Fluoride (NbO_2F). For Compound 5, the impurities are Potassium Niobium Fluoride ($K_2(NbF_7)$) and Potassium Niobium Oxide (KNb_3O_6). For Compound 6, the impurities are Potassium Molybdenum Oxide (K_2MoO_4 and K_4MoO_5). For Compound 7, the impurity is Potassium Niobium Fluoride (K_2NbF_7). For Compound 8, the impurity is Potassium Molybdenum Oxide (KMo_5O_{13}) and Potassium Molybdenum Oxide Fluoride ($K(MoO_3)_3F$).

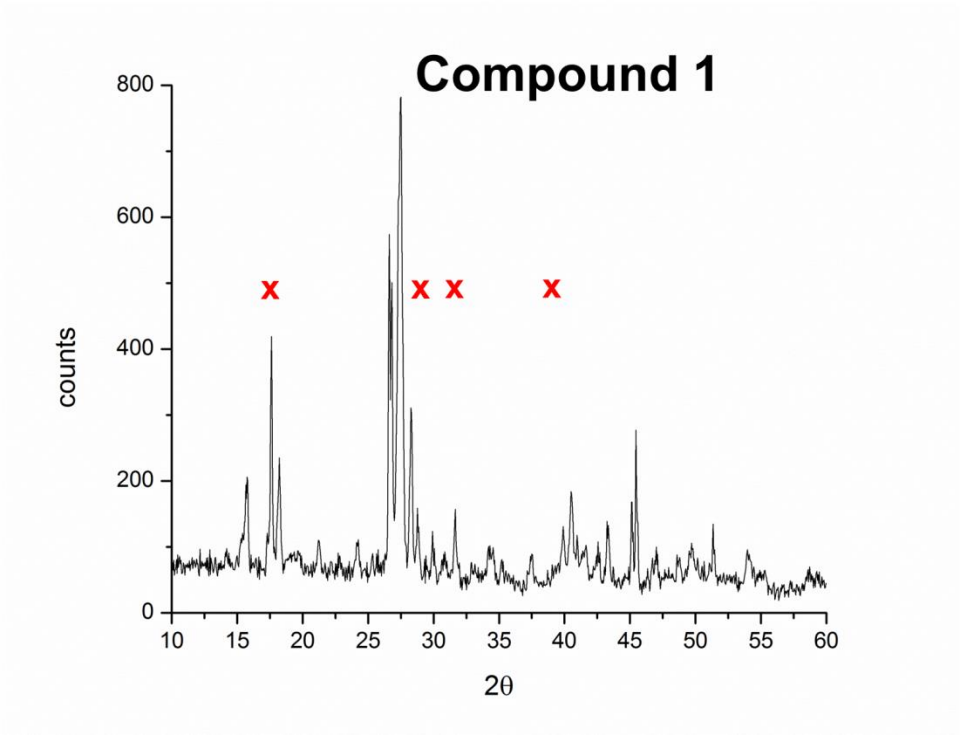
Compound 1
counts
2θ
0
200
400
600
800
10
15
20
25
30
35
40
45
50
55
60
x
x
x
x

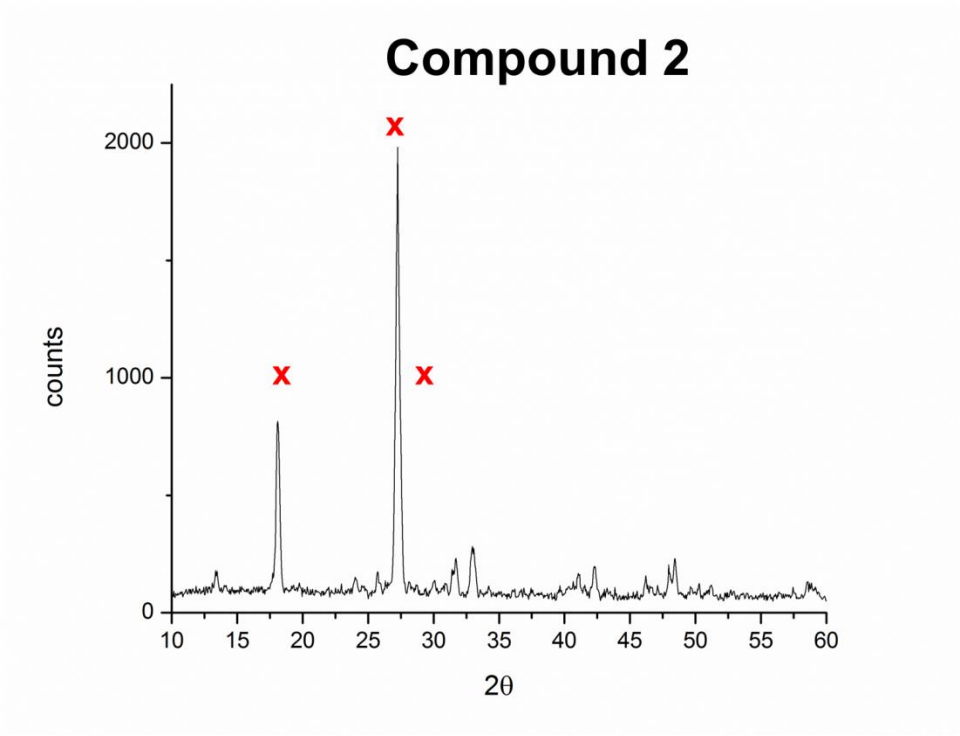
Compound 2
counts
2θ
0
1000
2000
10
15
20
25
30
35
40
45
50
55
60
x
x
x

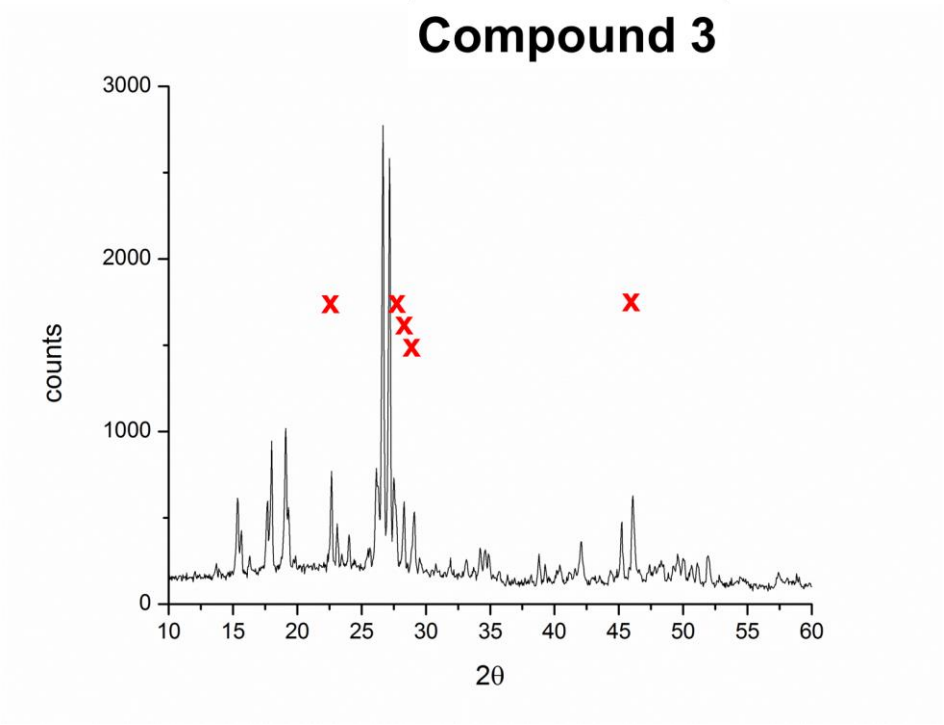
Compound 3
counts
2θ
0
1000
2000
3000
10
15
20
25
30
35
40
45
50
55
60

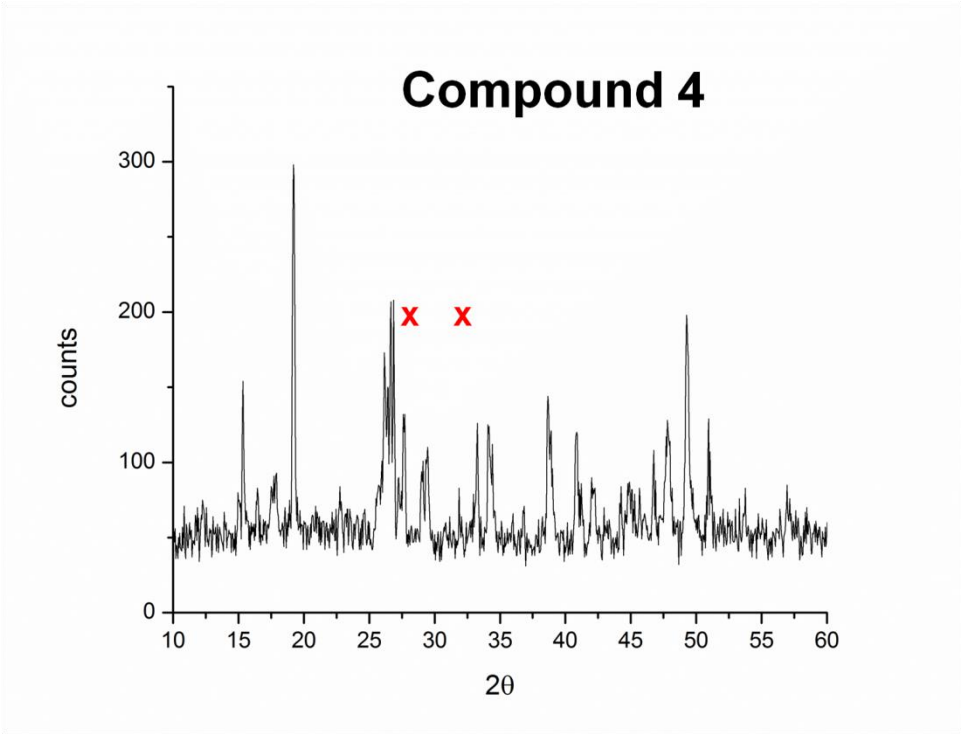
Compound 4
counts
2θ
0
100
200
300
10
15
20
25
30
35
40
45
50
55
60

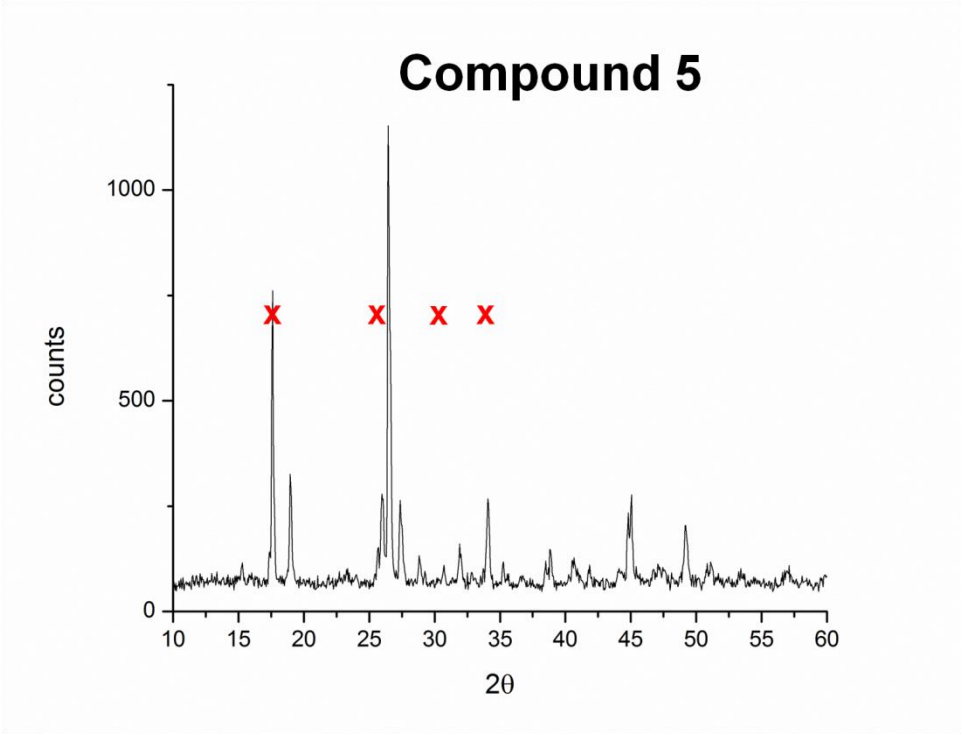
Compound 5
counts
1000
500
0
10
15
20
25
30
35
40
45
50
55
60
2θ

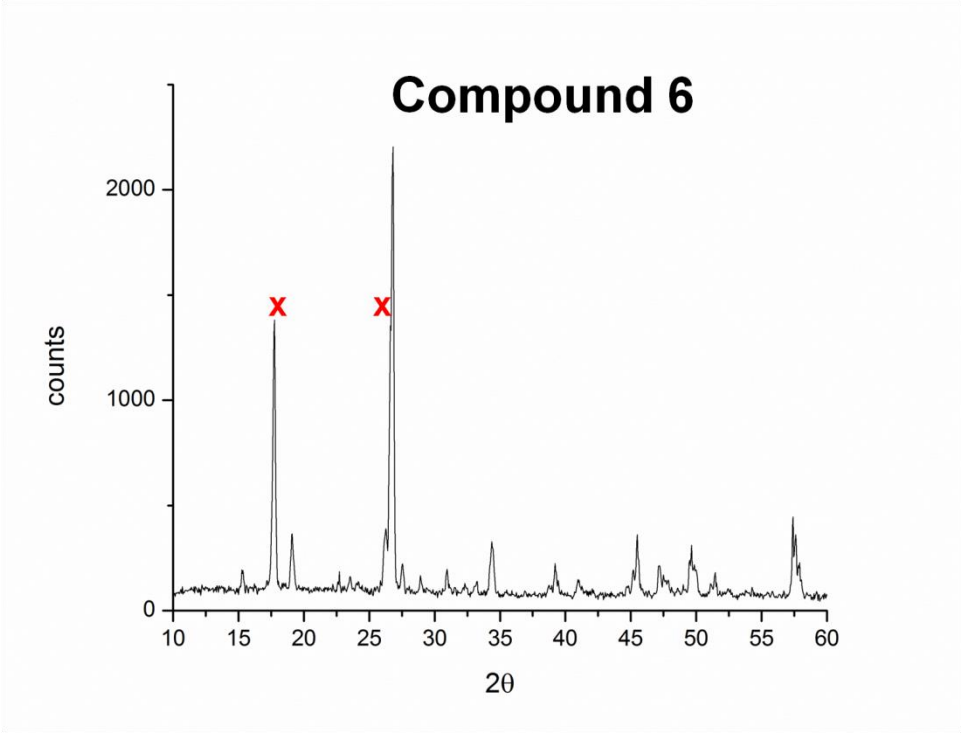
Compound 6
counts
2000
1000
0
10
15
20
25
30
35
40
45
50
55
60
2θ

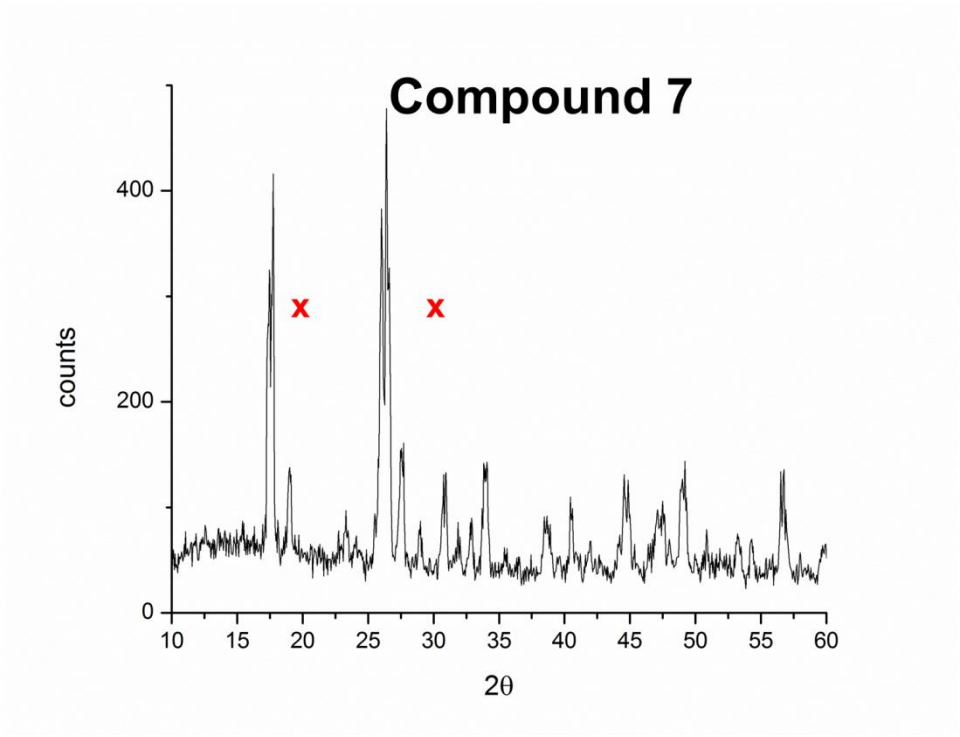
Compound 7
counts
2θ
x
x
0
200
400
10
15
20
25
30
35
40
45
50
55
60

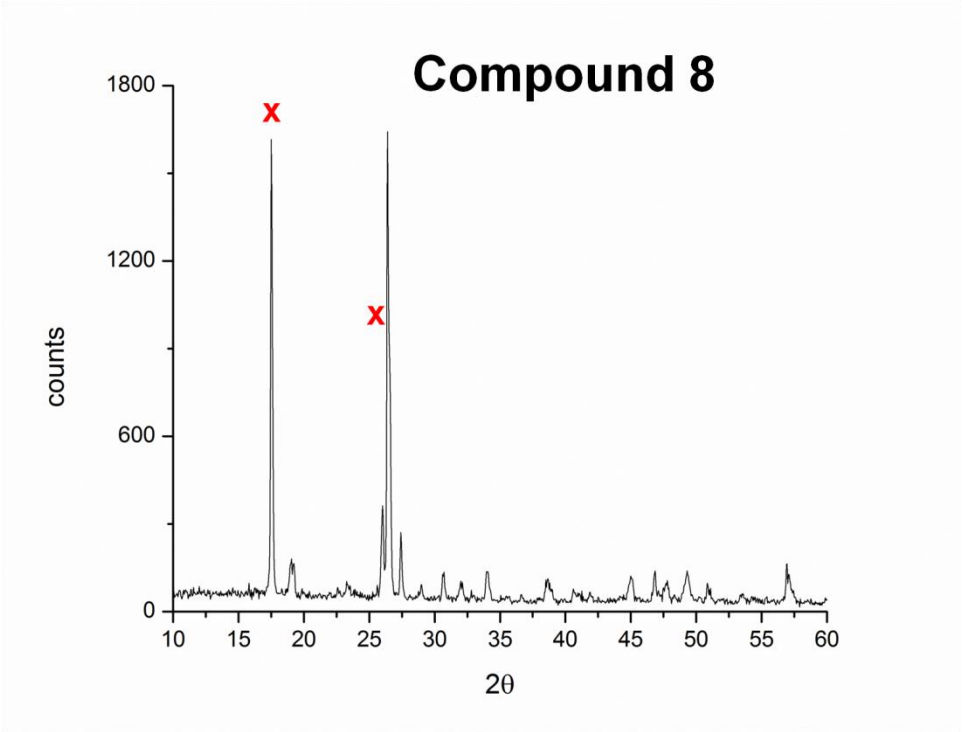
Compound 8
counts
2θ
x
x
0
600
1200
1800
10
15
20
25
30
35
40
45
50
55
60

4. Energy Dispersive X-Ray Spectrum Analysis of compounds 1-8 .

			Atomic % (found)						
Compound	X	M	K	M	O	F	X	Ratio X /M (found)	Ratio X /M (expected)
1	$Cl_{1/3}$	V	0.216	0.108	0.080	0.599	0.0060	**0.056**	**0.056**
2	$Br_{4/2}$	V	0.177	0.089	0.116	0.593	0.0252	**0.283**	**0.333**
3	Cl	Mo	0.192	0.120	0.232	0.435	0.0206	**0.172**	**0.167**
4	Br	Nb	0.174	0.123	0.099	0.585	0.0185	**0.150**	**0.167**
5	$Br_{4/2}$	Nb	0.166	0.100	0.105	0.600	0.0295	**0.296**	**0.333**
6	$Br_{4/2}$	Mo	0.178	0.123	0.194	0.465	0.0408	**0.332**	**0.333**
7	$I_{4/2}$	Nb	0.148	0.096	0.094	0.634	0.0284	**0.296**	**0.333**
8	$I_{4/2}$	Mo	0.164	0.106	0.168	0.529	0.0322	**0.303**	**0.333**

1.

			Atom % (expected)				
Compound	X	M	K	M	O	F	X
1	$Cl_{1/3}$	V	0.250	0.120	0.120	0.553	0.007
2	$Br_{4/2}$	V	0.244	0.118	0.118	0.529	0.039
3	Cl	Mo	0.250	0.120	0.240	0.420	0.020
4	Br	Nb	0.250	0.120	0.120	0.540	0.020
5	$Br_{4/2}$	Nb	0.244	0.118	0.118	0.529	0.039
6	$Br_{4/2}$	Mo	0.244	0.118	0.235	0.412	0.039
7	$I_{4/2}$	Nb	0.244	0.118	0.118	0.529	0.039
8	$I_{4/2}$	Mo	0.244	0.118	0.235	0.412	0.039

Individual Spectra of Compounds 1 – 8.

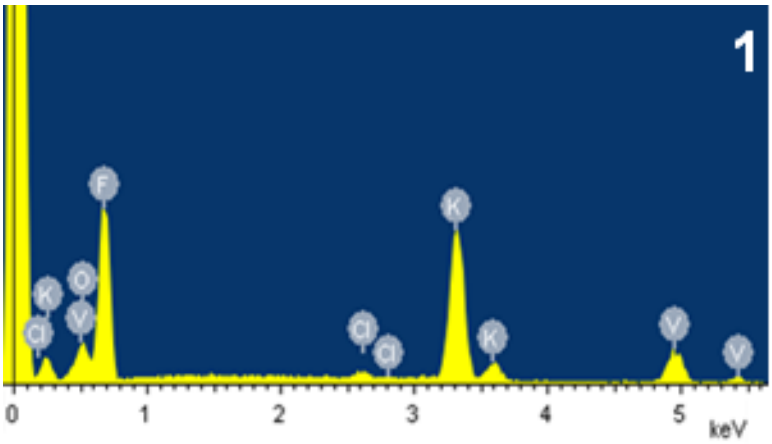

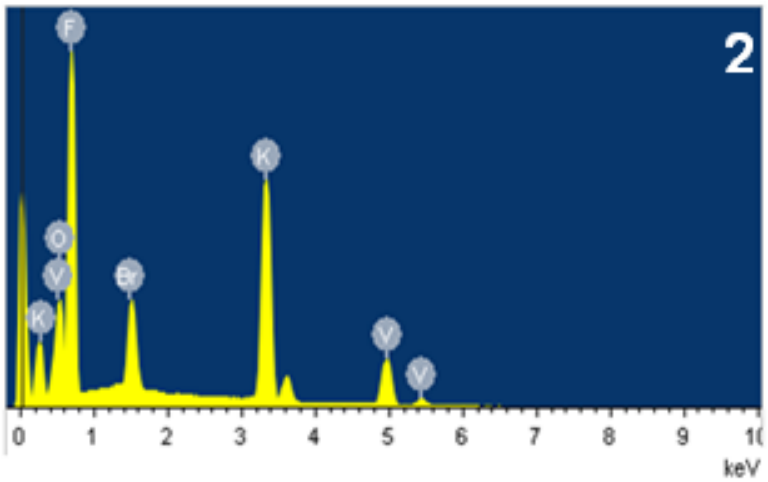

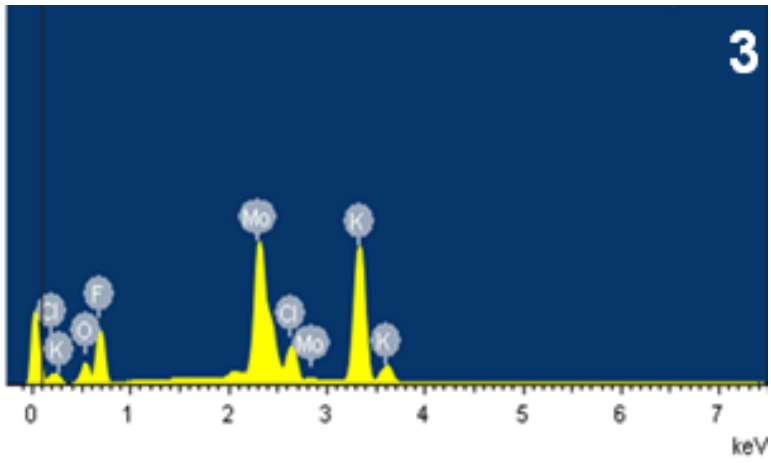

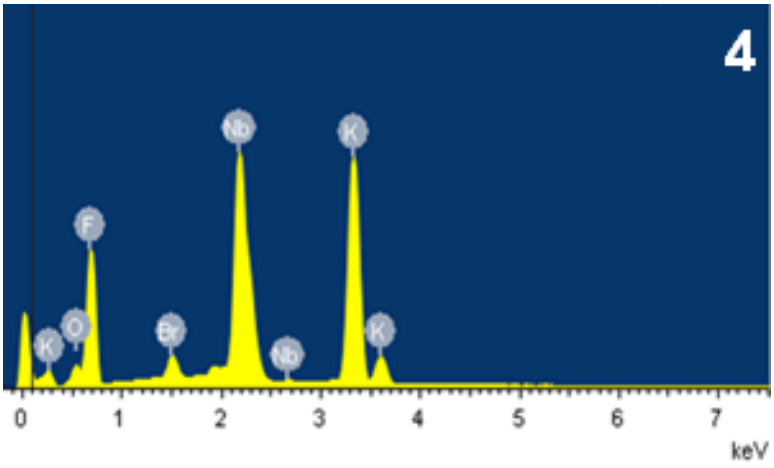
4
Nb
K
F
K
O
Br
Nb
K
0
1
2
3
4
5
6
7
keV

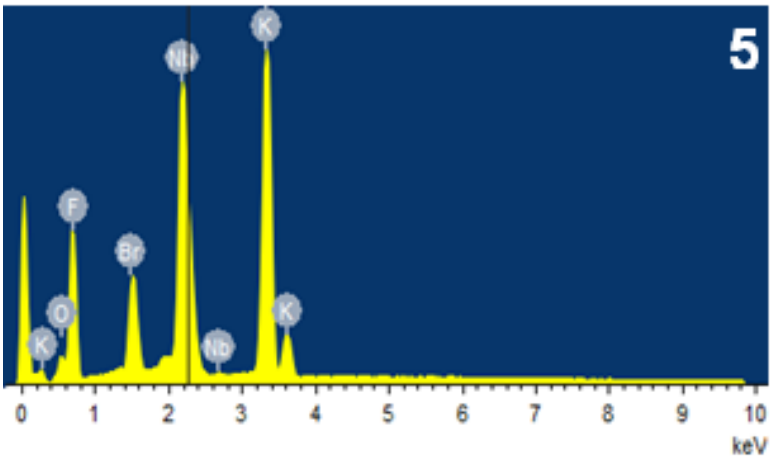
5
K
Nb
F
Br
O
K
Nb
K
0
1
2
3
4
5
6
7
8
9
10
keV

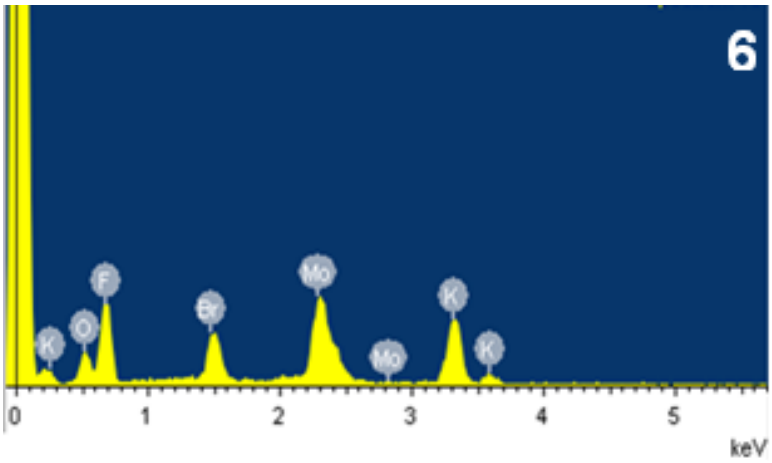
6
F
Mo
Br
K
K
O
Mo
K
0
1
2
3
4
5
keV

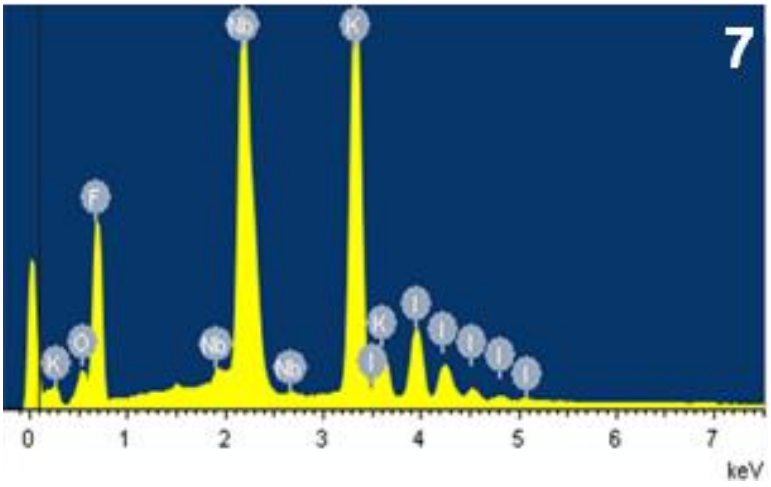
7
Nb
K
F
O
K
Nb
Nb
K
I
I
I
I
I
I
0
1
2
3
4
5
6
7
keV

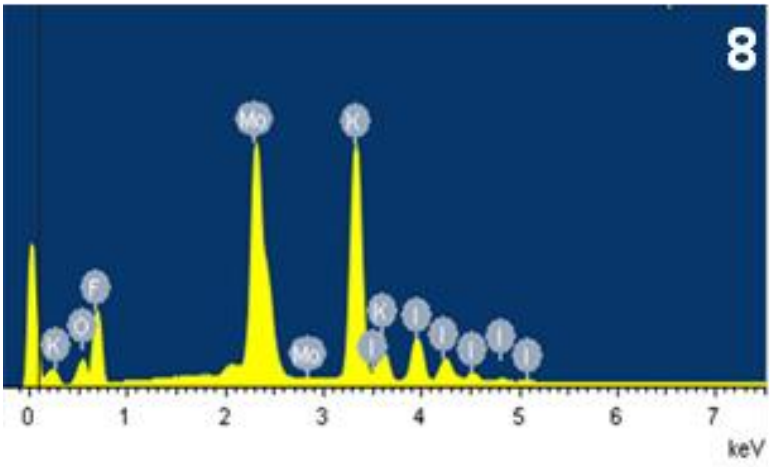
8
Mo
K
F
O
K
Mo
K
I
I
I
I
I
I
0
1
2
3
4
5
6
7
keV

5. Discussion of Halide Disorder in Channels.

During structural determination of the compounds, all had broad distributions of electron density within pores surrounded by potassium cations (see Figure S 1). This disorder was modeled with a single disordered halide for structures 1 – 4. Refinement was performed by splitting sites to isolate electron density as discretely as possible; however, the broadness frequently required elongated halide ellipsoids.

Structures 5 – 8 showed poor refinement with the use of a single halide ion: discrete sites decidedly refined to three sites of occupancies in the ratio of 1 : 0.5 : 0.5. These sites were modeled as a 50:50 combination of the moieities $[X_3]^-$ and $[X]^-$ (X = Br, I). The occupancies were initially freely refined, and then identified as . We note that $[Br_3]^-$ and $[I_3]^-$ ions were not used as starting reagents but must have been generated in situ; we attribute this oxidation during hydrothermal conditions.

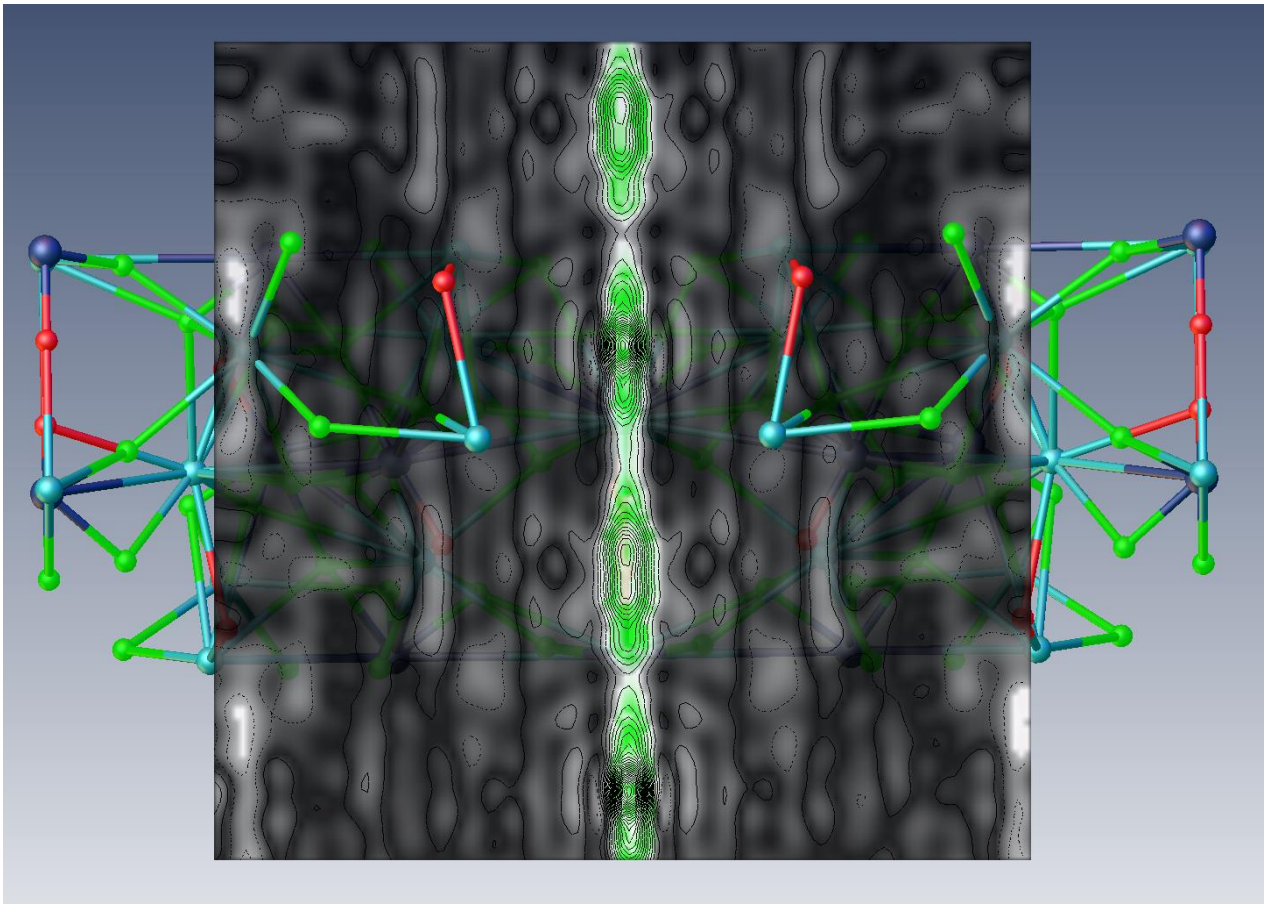

Figure S 1. A contour Fourier difference map of Compound 4 showing the broad distribution of electron density within the channels formed from potassium cations.

6. Commensurate Structural Solution for Compound 6.

Compound 6 showed a commensurate modulation of q = (0, 1/3, 0). We modeled it as a disordered structure and as a commensurately modulated, disordered structure. For comparison reasons, the main text describes the disordered structure; the commensurate structure is shown in figures S2 and S3.

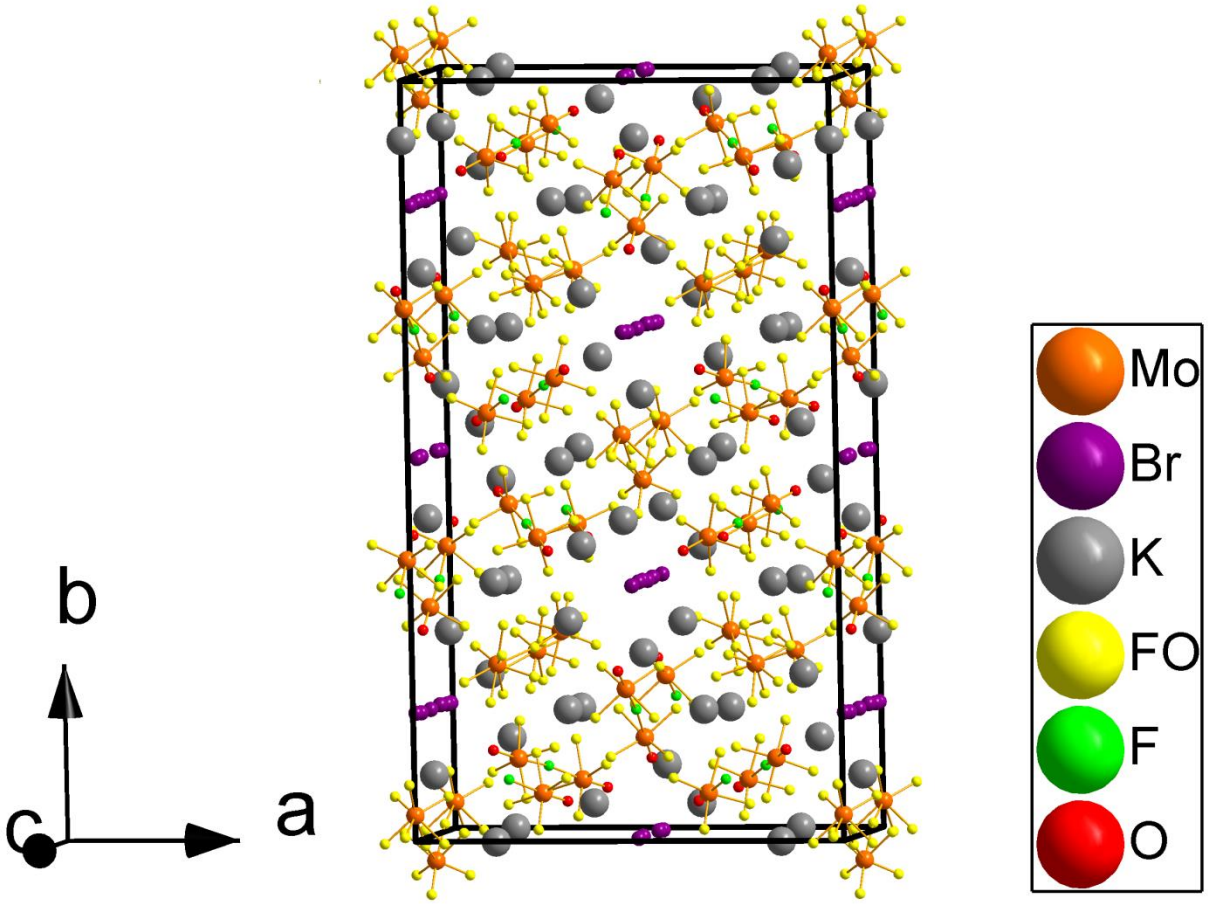

Figure S 2. A figure of the commensurate structure of Compound 6. The structure shows complicated disorder and separate channels that contain either bromide or tribromide anions.

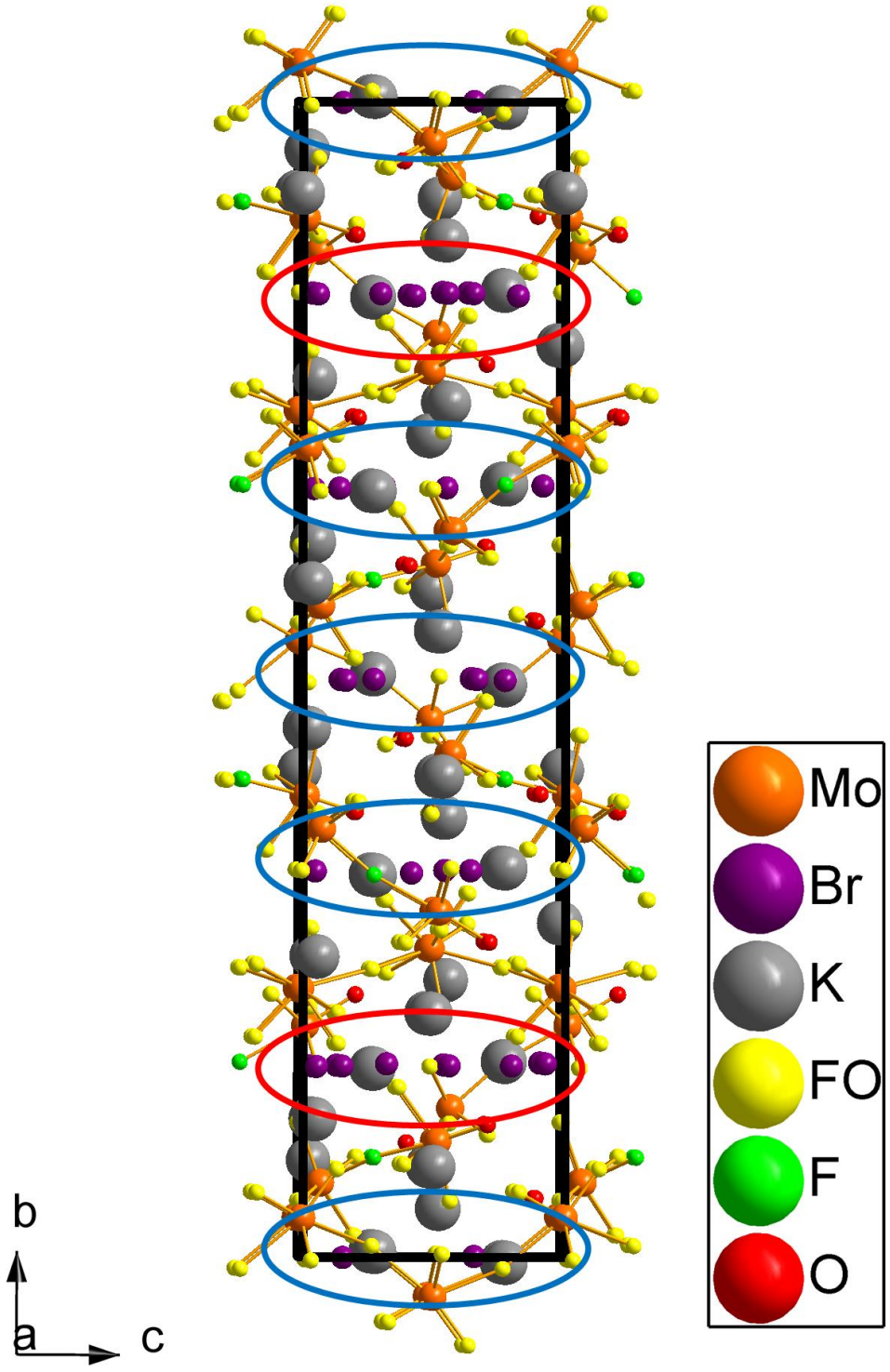

Figure S 3 A view of the bc plane of the commensurate structure of compound 6.
Blue ovals indicate channels of disordered bromide anions; red ovals indicate channels of disordered tribromide anions.

7. Explanation of the Λ Bend Observed in Compound 1.

The presence of two halide ion channel types introduces anisotropy that can allow for different bonding environments of the bridging fluoride anion. In this compound, the bond strength of K–X increases for $X=Cl^-$ as compared to $X = F^-$. The overall crystal packing thus places the Cl-K moeity closer to the bridging fluoride. This increases the resulting interaction K-F interaction to cause a Λ shape.

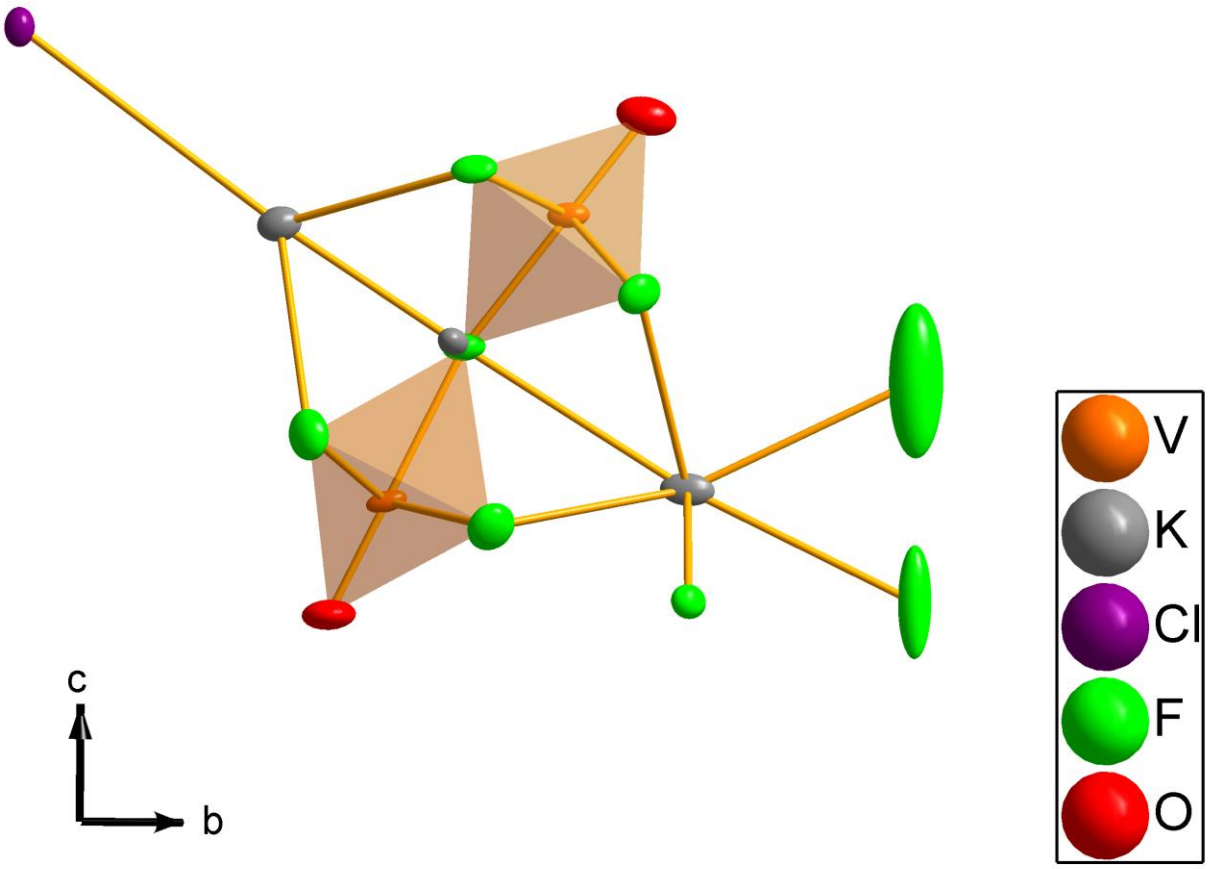

Figure S 4 The Λ-shaped unit of centrosymmetric $K_{10}(V_2O_2F_9)_3(F_2Cl)_{1/3}$.

8. Pair Distribution Function Analysis of Compounds 3 and 8.

Pair distribution function (PDF) measurements

PDF measurements were obtained at the 11-ID-B line at the APS at Argonne National Laboratory. Samples of Compound 3 and Compound 8 were placed within Kapton capillaries (1 mm diameter), and rotated during data collection. The PDF data were collected at 298 K with the rapid acquisition pair distribution function (RA-PDF) technique.[7] The data were collected with a Perkin-Elmer a α-Si detector and ~90 eV energy X-Rays (λ = 0.13702 Å). The data were combined and integrated within the program FIT2D.[8] Corrections were applied (before calculation of the PDF) for background, Compton, fluorescence scatter, geometric condsiderations, etc. within PDFGetX2.[9,10] Fits were performed within PDFGui by refinement of the unit cell parameters, scale factor, and delta1.

Fitting parameters for PDF data and resulting fitness.

Compound:	**3**	**8**
a(Å)	20.013787	20.22967
b (Å)	7.8307171	7.82105
c (Å)	11.27165	11.54426
scale factor	0.794625	0.72618
chisq	176.046	48.9983
red chisq	7.830717	0.004951
Rw	11.27165	0.23963

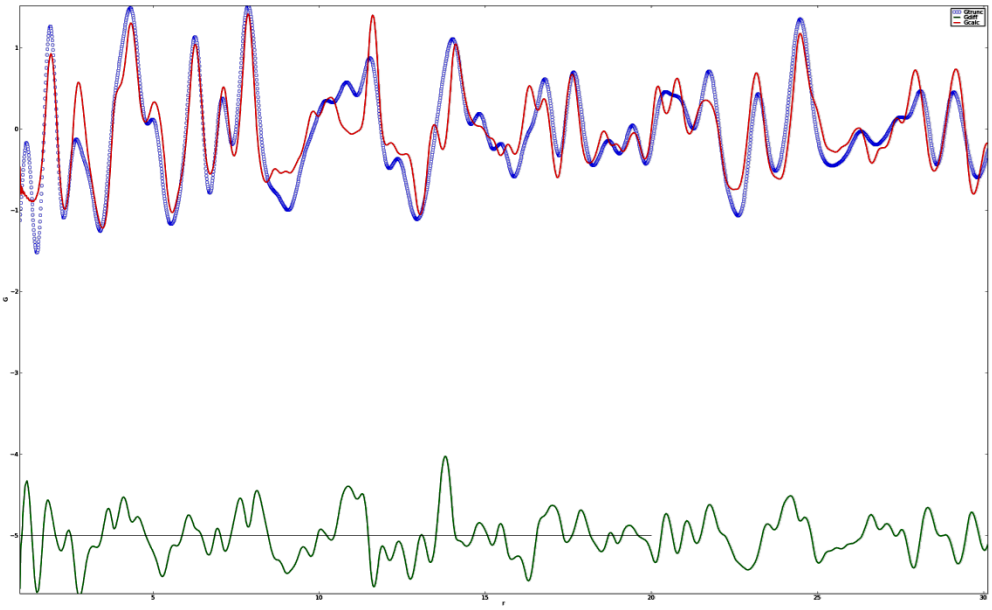

Figure S 5. a PDF fit from 1- 100 Å of Compound **3**: $K_{10}(Mo_2O_4F_7)_3Cl$ shown from 1 - 30 Å.

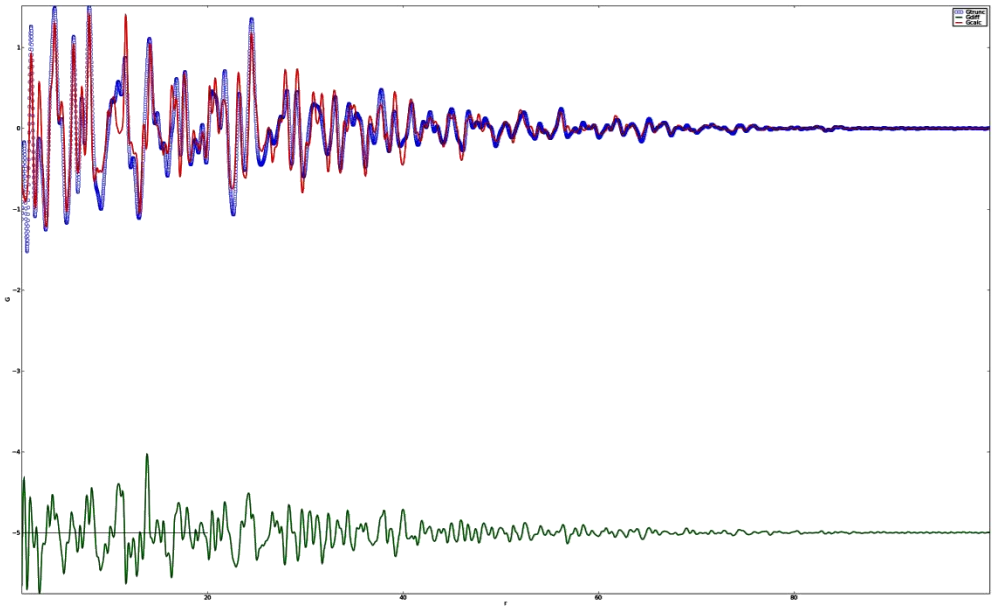

Figure S 6. A PDF fit from 1- 100 Å of Compound **3**: $K_{10}(Mo_2O_4F_7)_3Cl$ shown from 1 - 100 Å.

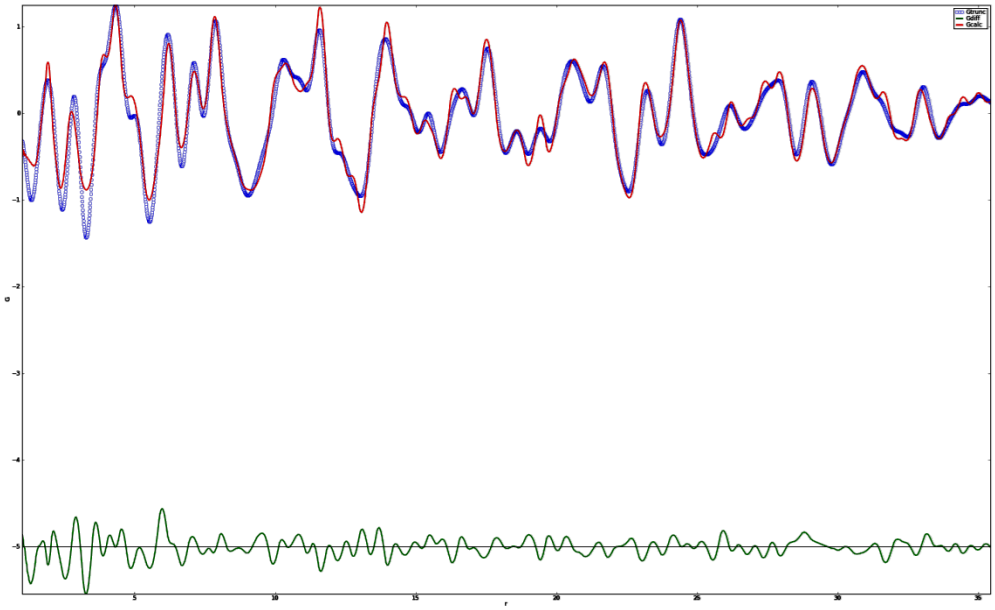

Figure S 7. A PDF fit from 1- 100 Å of Compound **8**: $K_{10}(Mo_2O_4F_7)_3I_{2/2}$ shown from 1 - 30 Å.

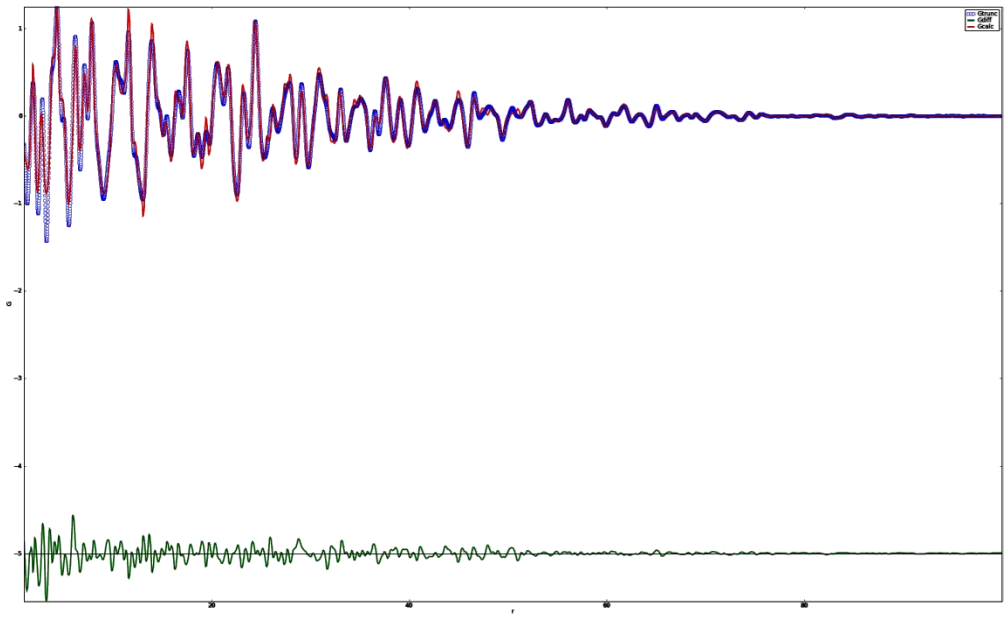

Figure S 8. A PDF fit from 1- 100 Å of Compound **8**: $K_{10}(Mo_2O_4F_7)_3I_{2/2}$ shown from 1 - 100 Å.

9. Computational Details and Coordinates of Input and Output Files for Geometry Optimizations.

For the computational experiments, Each pseudopotential defines a basis set to be used, which depends on the atom. The basis set references for each atom are in the table below, and at http://www.q-chem.com/qchem-website/manual_4-1.html#tth_sEc8.6.2.[11-15]

Table S 1. The basis sets used for each atom, depending on the pseudopotential used.

	CRENBL	LANL2DZ	SBKJC
F,O	Reference 7	Pople 6-31G basis used	Reference 8
Nb	Reference 9	Reference 10	Reference 11

Geometry optimizations were performed on the $[Nb_2O_2F_9]^{3-}$ anion in a) a linear bimetallic configuration constructed by use of the coordinates of the vanadium anion $[V_2O_2F_9]^{3-}$, but with alteration of niobium for vanadium, b) a Λ-shaped configuration with a slight perturbation of the bridging fluoride between the two transition metals, c) and of a Λ–shaped $[Nb_2O_2F_9]^{3-}$ made by use of the anion of $K_{10}(Nb_2O_2F_9)_3Br$ compound. All optimizations resulted in a linear $[Nb_2O_2F_9]^{3-}$ bimetallic unit.

Coordinates of Input files.

Linear $[Nb_2O_2F_9]^{3-}$ Input

Nb	10.17879	1.32782	2.34407
F	11.51709	2.21451	3.44745
F	11.54661	0.06524	1.75773
F	8.80628	0.05818	1.76097
F	8.83988	2.21098	3.44583
F	10.17950	0.00000	4.04820
O	10.17950	2.46840	1.04848
Nb	10.18021	-1.32782	5.75233
F	8.84191	-2.21451	4.64895
F	8.81239	-0.06524	6.33867
F	11.55271	-0.05818	6.33543
F	11.51912	-2.21098	4.65057
O	10.17950	-2.46840	7.04792

Perturbed Linear $[Nb_2O_2F_9]^{3-}$ Input

Nb	-0.0015769	1.4096715	-1.7656269
F	1.3747668	2.3649960	-0.7573341
F	1.3736230	0.2151727	-2.4743777
F	-1.3754440	0.2132403	-2.4730517
F	-1.3784500	2.3633491	-0.7564286
F	-0.1000013	0.0000001	-0.0000000
O	-0.0028490	2.4939025	-3.1244675
Nb	0.0015765	-1.4096715	1.7656269
F	-1.3747661	-2.3649986	0.7573352
F	-1.3736249	-0.2151752	2.4743789
F	1.3754422	-0.2132379	2.4730506
F	1.3784506	-2.3633463	0.7564274
O	0.0028530	-2.4939027	3.1244674

Λ Shaped $[Nb_2O_2F_9]^{3-}$ Input

Nb	0.00000	-4.49988	-3.13807
F	-1.35308	-5.64777	-3.92622
F	-1.39581	-3.82240	-1.95846
F	0.00000	-6.06395	-1.60237
O	0.00000	-3.27455	-4.30092
F	1.35308	-5.64777	-3.92622
F	1.39581	-3.82240	-1.95846
Nb	0.00000	-8.08590	-0.66934
F	-1.35512	-8.34548	-2.03759
F	1.35512	-8.34548	-2.03759
F	-1.34291	-7.25213	0.41310
F	1.34291	-7.25213	0.41310
O	0.00000	-9.63868	0.00698

Table S 2 below contains structural parameters for the optimized geometries of the $[Nb_2O_2F_9]^{3-}$ BBU, as a function of initial guess geometry (bent, linear, or perturbed as explained in text), pseudopotential (or effective core potential, ECP) and functional (M06, M11, PBE0, and TPSSH). The functionals were chosen to represent a range of methods: PBE0 is a GGA functional; TPSSH, M06, and M11 are meta-GGA functionals; and M11 is additionally a long-range-corrected functional. The optimized geometries are robust to the method used, except for two cases using the M06 functional (bolded rows in table).

The table below contains structural parameters for the optimized geometries of the $[Nb_2O_2F_9]^{3-}$ BBU, as a function of initial guess geometry (bent, linear, or perturbed as explained in text), pseudopotential (or effective core potential, ECP) and functional (M06, M11, PBE0, and TPSSH). The functionals were chosen to represent a range of methods: PBE0 is a GGA functional; TPSSH, M06, and M11 are meta-GGA functionals; and M11 is additionally a long-range-corrected functional. The optimized geometries are robust to the method used, except for two cases using the M06 functional (bolded rows in table).

Table S 2. This table demonstrates that the output optimized geometries of the $[Nb_2O_2F_9]^{3-}$ BBU are nearly independent of the basis and functional used. Only for two cases (bolded rows), both using the M06 functional, does the Nb-bridging F-Nb angle deviate more than one degree from perfect linearity. The last two rows show the average and standard deviations of the structural parameters; the second number in each cell is that quantity ignoring the contribution from the cases where the Nb-bridging F-Nb motif is nonlinear.

Starting geom.	ECP	Functional	Nb-F-Nb (°)	Nb-bridge F (Å)	Nb-axial F (Å)	Nb-O (Å)
bent	**CRENBL**	**M06**	**173.23**	**2.25**	**1.98**	2.78
bent	CRENBL	M11	179.13	2.23	2.00	2.78
bent	CRENBL	PBE0	179.79	2.25	1.98	2.78
bent	CRENBL	TPSSH	179.99	2.26	1.99	2.8
bent	LANL2DZ	M06	179.44	2.24	1.97	2.77
bent	LANL2DZ	M11	179.60	2.21	1.97	2.76
bent	LANL2DZ	PBE0	179.70	2.24	1.96	2.76
bent	LANL2DZ	TPSSH	179.82	2.24	1.97	2.78

bent	**SBKJC**	**M06**	**172.62**	**2.25**	**1.99**	2.78
bent	SBKJC	M11	179.93	2.23	2.00	2.77
bent	SBKJC	PBE0	179.77	2.25	1.99	2.78
bent	SBKJC	TPSSH	179.81	2.26	2.00	2.8
linear	CRENBL	M06	180.00	2.25	1.99	2.78
linear	CRENBL	M11	180.00	2.23	2.00	2.79
linear	CRENBL	PBE0	180.00	2.25	1.98	2.78
linear	CRENBL	TPSSH	180.00	2.26	1.99	2.8
linear	LANL2DZ	M06	180.00	2.24	1.97	2.76
linear	LANL2DZ	M11	180.00	2.22	1.97	2.76
linear	LANL2DZ	PBE0	180.00	2.23	1.97	2.76
linear	LANL2DZ	TPSSH	180.00	2.24	1.97	2.78
linear	SBKJC	M06	180.00	2.25	2.00	2.78
linear	SBKJC	M11	180.00	2.23	2.00	2.78
linear	SBKJC	PBE0	180.00	2.25	1.99	2.78
linear	SBKJC	TPSSH	180.00	2.26	2.00	2.8
perturbed	CRENBL	M06	179.38	2.25	1.99	2.78
perturbed	CRENBL	M11	179.65	2.24	2.00	2.79
perturbed	CRENBL	PBE0	179.51	2.25	1.99	2.78
perturbed	CRENBL	TPSSH	179.52	2.26	1.99	2.8
perturbed	LANL2DZ	M06	179.38	2.24	1.97	2.76
perturbed	LANL2DZ	M11	179.73	2.22	1.97	2.77
perturbed	LANL2DZ	PBE0	179.50	2.24	1.97	2.76
perturbed	LANL2DZ	TPSSH	179.47	2.24	1.97	2.78
perturbed	SBKJC	M06	179.33	2.25	2.00	2.78
perturbed	SBKJC	M11	179.52	2.23	2.00	2.78
perturbed	SBKJC	PBE0	179.57	2.25	1.99	2.78
perturbed	SBKJC	TPSSH	179.63	2.26	2.00	2.8

Average			179.36/179.74	2.24/2.24	1.99/1.99	2.78/2.78
Std. deviation			1.60/0.26	0.01/0.01	0.01/0.01	0.01/0.01

All Q-Chem input and output files, along with a script to generate and submit the Q-Chem jobs, are included in the file Nb_optimizations.zip.

10. References

(1) Burns, G. R.; Renner, R. M. *Spectrochimica Acta Part a-Molecular and Biomolecular Spectroscopy* **1991**, *47*, 991.

(2) Kalina, D. W.; Lyding, J. W.; Ratajack, M. T.; Kannewurf, C. R.; Marks, T. J. *Journal of the American Chemical Society* **1980**, *102*, 7854.

(3) Świetlik, R.; Schweitzer, D.; Keller, H. J. *Physical Review B* **1987**, *36*, 6881.

(4) Trotter, P. J.; White, P. A. *Applied Spectroscopy* **1978**, *32*, 323.

(5) Chen, X.; Rickard, M. A.; Hull, J. W., Jr.; Zheng, C.; Leugers, A.; Simoncic, P. *Inorg Chem* **2010**, *49*, 8684.

(6) Iqbal, Z.; Baughman, R. H.; Kleppinger, J.; Macdiarmid, A. G. *Solid State Communications* **1978**, *25*, 409.

(7) Chupas, P. J.; Qiu, X.; Hanson, J. C.; Lee, P. L.; Grey, C. P.; Billinge, S. J. L. *Journal of Applied Crystallography* **2003**, *36*, 1342.

(8) Hammersley, A. P.; Svensson, S. O.; Hanfland, M.; Fitch, A. N.; Hausermann, D. *High Pressure Research* **1996**, *14*, 235.

(9) Egami, T.; Billigne, S. J. l. *Underneath the Bragg peaks: structural analysis of complex materials*; Pergamon Press: Oxford, England, 2003.

(10) Qiu, X.; Thompson, J. W.; Billinge, S. J. L. *Journal of Applied Crystallography* **2004**, *37*, 678.

(11) Fernandez Pacios, L.; Christiansen, P. A. *The Journal of Chemical Physics* **1985**, *82*, 2664.

(12) LaJohn, L. A.; Christiansen, P. A.; Ross, R. B.; Atashroo, T.; Ermler, W. C. *The Journal of Chemical Physics* **1987**, *87*, 2812.

(13) Hay, P. J.; Wadt, W. R. *The Journal of Chemical Physics* **1985**, *82*, 299.

(14) Stevens, W. J.; Basch, H.; Krauss, M. *The Journal of Chemical Physics* **1984**, *81*, 6026.

(15) Stevens, W. J.; Krauss, M.; Basch, H.; Jasien, P. G. *Canadian Journal of Chemistry* **1992**, *70*, 612.